PROCEEDINGS OF ECOS 2023 - THE 36TH INTERNATIONAL CONFERENCE ON
EFFICIENCY, COST, OPTIMIZATION, SIMULATION AND ENVIRONMENTAL IMPACT OF ENERGY SYSTEMS
25-30 JUNE 2023, LAS PALMAS DE GRAN CANARIA, SPAIN

Detailed Modeling Framework for Integrated Photovoltaic in Partial Shading Conditions

Justin McCarty[a,b], Christoph Waibel [a], Arno Schlueter[a]

[a] *Chair of Architecture and Building Systems, ETH Zurich, Switzerland*
[b] *corresponding author mccarty@arch.ethz.ch*

Abstract:

Building integrated photovoltaic (BIPV) systems are a crucial component of the transition to a low-carbon energy system. However, current simplified models of PV cells and modules used in building and urban energy simulations may not accurately capture the performance of various PV technologies under partial shading conditions. In this paper, we propose a novel framework for modeling parametric BIPV arrays using a high-resolution irradiance grid and a power model that operates from the evaluation of IV-curves at the cell level to the AC to DC conversion in the inverter. This allows us to combine PV modules of varying sizes and electrical configurations based on the selected inverter type, and to capture the operative benefits of multiple types of cell technologies, module designs, and electrical layouts in building-based PV applications. We evaluate the proposed framework by comparing its performance to measurement data and to three other frameworks found in the literature through the simulation of two BIPV façades and a tilted rooftop array. The results show that the proposed framework is necessary to account for partial shading (if present) as well as provide operative details when the type of inverter to be used is in question. Overall, this paper presents a novel framework for modeling the performance of PV cells and modules in building and urban energy simulations, which has significant implications for the design and optimization of building-based PV systems.

Keywords:

Integrated PV, BIPV, Partial Shading, Simulation, Urban.

1. Introduction

Photovoltaics (PV) are becoming increasingly common elements of building and urban energy systems research and optimisation [1, 2, 3]. However, we find that much of the research employs coarse level performance modeling frameworks to parameterise expected PV output. Current standards within research rely on low resolution irradiance estimations and simplistic conversion efficiency methods. These models were originally developed for PV systems that were largely unobstructed and used standard PV modules, such as the arrays found in utility-scale ground mount systems and on rooftops. However, the low cost of PVs and the need for rapid urban energy decarbonisation is leading to their use in environments where the boundary conditions are less than ideal. Due to high degrees of partial shading, heat, and the need for custom module sizing many systems may be installed and produce lower overall system efficiencies than envisioned during planning. This has the potential to translate into less realistic assessments of lifecycle cost and carbon performance at the system scale and grid stability and energy availability at the urban scale. Towards the goal of reducing the performance gap for building and urban energy systems research we compare the results of different PV performance modeling frameworks.

1.1. Objectives

In this paper we demonstrate that a highly detailed performance model can help modelers understand the potential loss in an urban PV system. Additionally, we show that the high level of resolution may not always be necessary and is dependent on the context of the geometry model (i.e. the spatial context of the surface being evaluated). We describe a proposed modeling framework compiled from the literature, compare an initial set of simulated performance indicators from the proposed framework to measured data sets. Then we apply the proposed framework to several theoretical building integrated PV (BIPV) arrays; two façade arrays and one tilted rooftop array. The results of these simulations will be compared to three common frameworks to modeling BIPV performance, briefly described in Table 1. We compare the results in terms of modeling effort and calculated PV yield and outline in which context which modeling resolution is best suited.

1.2. Research Questions and Hypotheses

We ask the following questions with proposed hypotheses for help guide the reporting of the research:

https://doi.org/10.52202/069564-0306

Framework	Description
Surface Face	The surface is divided by a single grid dimension and the center points of each resulting face are used for irradiance simulations. Power is then extracted using a simple power conversion model from the irradiance of the sensor point and the area of the face.
Module Center	The surface is divided by a BIPV array. The center point of the resulting modules are used for irradiance simulations. Power is then extracted using a simple power conversion model from the irradiance of the sensor point and the area of the module.
Cell Center	The modules created by the Module Center framework are further divided into cells. The center point of the resulting cells are used for irradiance simulations. Power is then extracted using the power conversion model from the irradiance of the sensor point and the area of the cell.
Cell IV	The center point of the cells from the Cell Center framework are used for irradiance simulations. Power is then extracted using a single-diode equivalent circuit model from the irradiance of the sensor point and parameters of the selected module/cell.

Table 1: Descriptions of the four modeling frameworks used in the paper.

- Does the proposed framework produce accurate results?
    - Evidence in the literature suggests that the proposed framework is a viable method of predicting the yield of all module types. We aim to improve upon existing methods to bring more flexibility to the framework and providing further clarification of when a more detailed method should be applied over simpler methods.
- In what situations is it recommended to use the proposed framework over simpler methods (e.g. NOCT or performance ratio)?
    - We suspect that surfaces that are subject to mostly diffuse light or mostly direct light are candidates for the simpler methods, while those that see a mixture of direct and diffuse light will not be accurately characterised by these methods and require the more detailed method described in this paper. We expect to see results diverge the most between the *Cell IV* and the other frameworks for the façades while the rooftop arrays will be more consistent between the frameworks.

2. PV Modeling Frameworks

We define a PV performance modeling framework as a set of models and protocols that assist modelers in assessing the power output of a PV array from the definition of the surface to the calculation of performance indicators such as self-consumption (PVSC, i.e. how much of generated electricity is consumed). A framework has three components:

1. Definition of the array geometry through the discretization of a surface.
2. Simulation of the effective irradiance (G_{eff} [$\frac{\text{W}}{\text{m}^2}$]) on the array surfaces.
3. Conversion of the G_{eff} to power (P [W]), either in direct-current (P_{DC}) or alternating current (P_{AC}), typically expressed per timestep which is usually in hours, thus Watt-hours (Wh).

In the following sections we provide a review of the various PV performance modeling frameworks summarised in Table 1. The first group, discussed in Section 2.1. are often found in the literature, vary in their degree of spatial resolution, and utilise one of several power conversion methods. There are often functions of efficiency and performance ratio, to convert G_{eff} into P_{DC}. After reviewing these methods we introduce, in Section 2.2. the proposed high-resolution framework that we have compiled from several sources in the literature. This framework relies on detailed spatially accurate models of module and cell placement, as well as high accuracy irradiance simulations. The power conversion model is a single-diode equivalent circuit model from Bishop (1988) [4] to characterise the electrical attributes of each cell before merging them system wide. It is commonly applied in a less spatially resolute context (i.e. module center points) in power systems modeling for large unobstructed PV arrays.

2.1. Existing module and surface based modeling approaches

The yield from a PV cell is, at its most basic level, a function of the solar irradiance of the cell and the cell's ability to act as a semiconductor through the photovoltaic effect to convert this energy into an electrical charge. In practical terms for a modeling framework this can equate to simply multiply G_{eff} of a module by an efficiency (η) factor associated with the module. This simple conversion can enable very rapid assessment frameworks. Rapid rooftop assessment platforms such as Google's Project Sunroof or Mapdwell have been in place for nearly a decade and rely on a combination of photogrammetry and often proprietary algorithms to estimate the shading on a roof due to nearby objects such as trees or buildings. While these tools do allow individuals to assess their rooftop PV potential quickly and with little to no barriers beyond data availability in their own region. While accessible these tools are not extensible to facades and results for the same location vary greatly between models, suggesting a high degree of inaccuracy is present [5]. In Switzerland a public tool called Sonnenfassade [6] exists for any building in the countries database of 3D models and quickly calculates irradiance using a performance ratio (PR) approach It uses this 3D model of a building along with local climatic data and a shade horizon profile built up of nearby mountains, hills, buildings, and vegetation to estimate the average yearly irradiation value in the middle point of the building's façades. This is then multiplied by the façade area and a PV PR of typically 80% to determine an annual potential yield value.

This was improved upon by Saretta et al. (2020) [7] due to a core inability in distinguishing potential windows and balcony type projections on the façade. The update equation uses three reductions factors to more accurately account for facade area based on a statistical database connected the the building age and type.

While more spatially accurate this approach still relies on the *PR* variable which is difficult to calculate without measured data of a similar system or an accurate model of the system. Additionally, a system's PR varies with time and when considering the dynamics of grid pricing and storage is a key parameter to understand. A temporally resolved approach exists in [8, 9], which employs similar methods to characterise potential irradiance, but does so for each hour of the year through the input of Typical Meteorological Year (TMY) weather data and angular modifiers to model reflection on the glass surface of a PV module. Other models exist as well such as Huld's modification of King's model [10] or the PV Watts method [9]. These methods employ more advanced methods of calculating output from the PV cell that are temperature dependent. To calculate module temperature (T_{mod} [°C]) the nominal operating cell temperature (*NOCT* [°C]) model is often employed [11], shown in Eq. 1, where *NOCT* is a parameter typically given on PV module data sheets and T_{air} ([°C]) is the ambient air temperature, and G_{eff} must be given in $[\frac{\text{mW}}{\text{cm}^2}]$.

$$T_{\text{mod}} = T_{\text{air}} + \frac{NOCT - 20}{80} \cdot G_{\text{eff}} \tag{1}$$

While these models employ more complexity to characterise module performance through various uses of cell temperature, but do not increase the level of detail used for calculating G_{eff}. This increase in spatial resolution can be found in the models employed in urban and building energy modeling tools such as in Fonseca et al. (2016) [12] and Waibel et al. (2017) [13]. These approaches use 3D scenes to simulate irradiance on any number of sensor points. In the former surfaces are discretized using a small amount of sensor points, typically 2-5 m^2 per sensor points, to reduce computation time. Daysim [14], a form of the validated lighting simulation engine Radiance [15], is then used to conduct ray tracing for the sensor points, taking into account any obstructions in the scene along with their reflectivity and transparency. The received irradiance is then used with a variation of Eq. 2 to calculate the yield for an hour of the day. Here G_{STC} is the irradiance during standard test conditions (STC) and $P_{\text{DC,STC}}$ [W] the power output. Similarly the latter framework uses ray tracing and view factors to rapidly assess potential irradiance on a sensor point and use it as input to a variation of Eq. 2.

$$P_{\text{DC}} = \frac{G_{\text{eff}}}{G_{\text{STC}}} \cdot P_{\text{DC,STC}} \left(1 + \gamma \left(T_{\text{mod}} - T_{\text{ref}}\right)\right) \tag{2}$$

These methods improve upon the spatial resolution of the irradiance gathering portion of a necessary PV performance modeling framework, but do not necessarily allow modelers to look at the performance of an array from a module-specific perspective, as they still rely on generic parameters for the type of cell. For module-specific calculations a method such as that employed in EnergyPlus [16] is necessary. The Sandia Performance Model (SPM) [17], utilises module and cell specific parameters to characterise the performance of the module being examined. It is also extended into a larger ecosystem of arrays and systems to account for transmission loss, inverter loss, and other factors such as maintenance to provide a value for system-wide grid-ready power $P_{AC,sys}$. The limitation is that while the SPM uses a cell-based approach of sorts it does not record the current-voltage (IV) curve of the module, just the output power for a timestep. This makes assessing its performance within a larger electrical topology such as a central or string inverter based system difficult as one needs to be able to calculate the maximum power point (MPP) that would come from the inverter or maximum power point tracking device (MPPT).

https://doi.org/10.52202/069564-0306

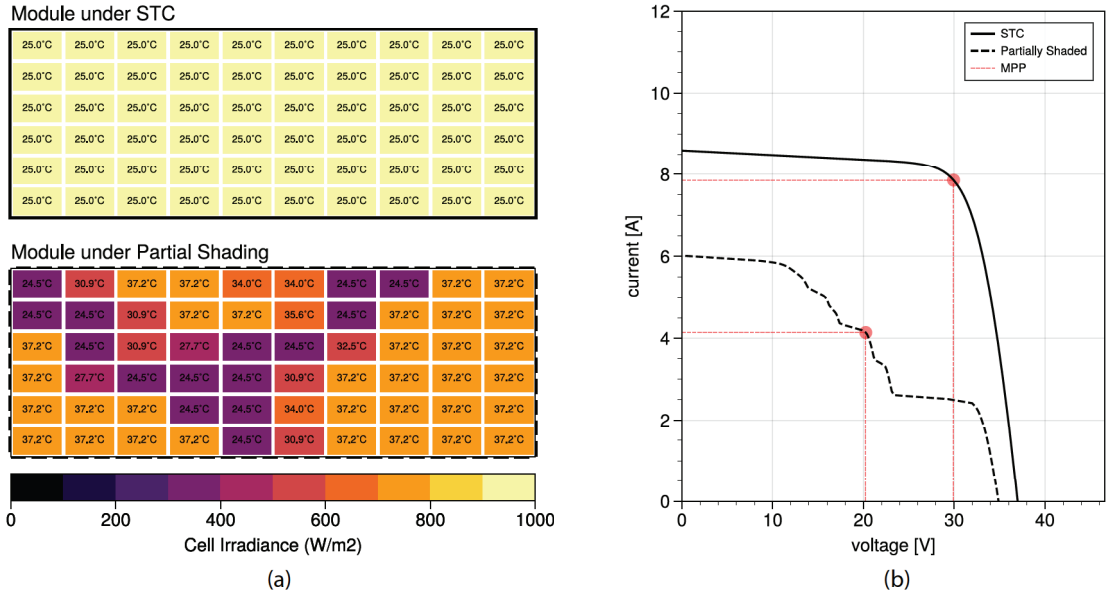

Figure 1: An example of a module under the partial shading of a tree branch (a) and its impact on the IV-curve and power output (b) as compared the a module under standard test conditions. These results were calculated using the proposed framework.

2.2. Existing cell based modeling approaches

When a module is partially shaded, as shown in Figure 1, it operates below optimum. This is due to unshaded cells (high current) reverse-biasing shaded cells (low current) in a string, which leads to overheating in the shaded cells and potential damage, referred to as mismatch. This is mitigated by bypass diodes to reduce the risk of catastrophic failures, but at the expense of total output. It is therefore vital to parameterise these effects in models of PV arrays if they are expected to operate under conditions with a great deal of partial shading. Furthermore, new module types, such as half-cut modules employ less straightforward configurations of cell arrangement and BIPV modules are typically highly customised such that contextualising the cells in module not only in their series placement but also in parallel is necessary to entirely account for the location of bypass diodes.

Additionally, specifying the type of electrical topologies as a part of the modeling framework is necessary to account for the entire impact of partial shading on system performance[18, 19, 20, 21]. This is due to the way in which current and voltage are accumulated when the IV curves of the cells and modules do not match.

Therefore, a highly detailed modeling framework should be able to model the impact of partial shading on a bespoke module's performance as well as throughout a larger electrical topology. Meyers et al. (2017) [22] and Chaudhari et al. (2018) [23] describe a modeling framework for characterising the mismatch in PV cells and modules to better account for partial shading on systems. Walker et al. (2019) [24] developed a workflow to simulate PV modules using a cell-based approach that begins from simulating the irradiance on the cell or an even finer resolution.

Both of the above approaches employ techniques for characterising cell performance that are crucial for modules under highly uneven irradiance such as reverse bias and bypass diodes. Additionally, modelers may want to study arrays with different sized modules (which is common in BIPV design) or explicitly model changes to modules such as front covers for aesthetics, or different bypass diode configurations during parametric optimisation.

3. Methodology, Data, and Tools

In this section we describe the models and methods used to conduct our comparative analysis of PV performance modeling frameworks.

First, we then describe the measured PV yield data (Section 3.1.) to which we compare the proposed framework. For the simulations we use a common monocrystalline module type, Sharp Solar 235Wp (Sharp-NU-U235F2). It was selected due to the availability of its parameters in the California Energy Commission's module

database [1] and it is the sole module found in the measured data. Then, in Section 3.2. the two 3D models that contain the façades and rooftop arrays which we use to compare the performance of the modeling frameworks are described. Then, the four modeling frameworks are summarised. The first (Section 3.3.) is currently common within the literature and employs simpler methods and lower levels of details than the third (Section 3.6.), which is the framework which we are proposing. We also describe the two other levels of detail that operate between these two methods that improve on the spatial resolution of the first, but utilise the same power conversion model; *Module Center* in Section 3.4. and *Cell Center* in Section 3.5..

3.1. Measured Datasets

We use a sub array from a rooftop installation at the United States of America National Institute of Standards and Technology (NIST) to evaulate the performance of the proposed modeling framework's power conversion model. The dataset for the sub array (SC3) is reported on in detail by Boyd (2015) [25]. It contains minute averages for a variety of sensors placed throughout a large rooftop array. The dataset was chosen for its availability and clean data. Ideally the dataset to compare against would be one that is vertically oriented and subject to partial shading. However, to the knowledge of the authors this does not exist. The array comprises of 84 modules of the module mentioned in Section 3.. Of the 84 modules there are seven strings of 12 modules that are combined in parallel to create a single DC output stream. The recorded data from this output was resampled into hourly data and compared against the IV-curve based framework. For the input G_{eff} and T_{cell} we rely on the measured data from within the array. G_{eff} comes from a single silicon reference cell in the array. T_{cell} is a mean value gather from several back-of-module sensors throughout the array. We evaluate the model results using mean absolute error (MAE) and a qualitative comparison of the result distribution.

3.2. 3D Building Geometry

We conduct a comparative analysis between the proposed framework (i.e. *Cell IV*) and the frameworks from the literature to describe the differences in their output and identify situations in which it may not be worth the computational cost of the more detailed method. To make the analysis more relevant to a broader audience we identify two Representative façades to simulate through a clustering analysis of buildings in a district in Zurich Switzerland. A third surface was added as well to compare a minimally obstructed rooftop situation. Clustering was done on building morphology metrics extracted from the urban region following Biljecki et al. (2022) [26]. Principal Component Analysis (PCA) was used to reduce the parameter space before applying a K-Medoids clustering process.[2].

Clustering returned three archetypal buildings, for which the southern-facing façades were extracted. On one of the buildings the extracted façade was unobstructed and it was decided to remove this from the analysis, leaving the two buildings and façades shown in Figure 2. The upper roof section of Building B was used for the roof analysis, where a 30° tilt facing south was assigned to the array. The buildings were modeled in a Rhino/Grasshopper [27] 3D environment and a script was developed to add BIPV and rooftop module arrays with each cell parameterized based on a landscape orientation of the PV module in the NIST dataset. Nearby opaque context was modeled with a 20% reflectivity. A tree exists near one of the residential buildings. This was modeled following Peronato et al. (2018) [28]. The scenes were used for ray-tracing to gather annual irradiance profiles with hourly timesteps.

3.3. Surface-based framework

The existing approach for urban-scale analysis of photovoltaics is to evaluate one or several sensor points on a facade and use those as the basis for the power conversion model. The surface's are discretized using a moderate resolution of two meters between each sensor point to reduce possible error to a negligible amount, as recommended by Peronato et al. (2018) [28]. We remove the area where the window faces intersect with the discretized grid cells to accurately account for the area available to potential PV. In the case of the rooftop array, the flat surface of the roof was split into faces and the center points were assigned the surface normal that would be associated with tilted modules, instead of rotating the faces themselves.

Typically the irradiance simulation would only be done for the sparse sensor points on the surface being analysed. However, due to the stochastic nature of the Radiance engine we use the irradiance map created for the cell-based approach described in a later section. For this we simply take the mean value of the three nearest points to each sensor point on the surface. This irradiance value, for both direct (G_{dir}) and diffuse irradiance (G_{diff}), is used to calculate G_{eff} using Eq. 4 and Eq. 3.

G_{dir} and G_{diff} are simulated for each sensor point using the enhanced 2-Phase ray-tracing method found in Subramanian (2017) [29] using Radiance.[3] They can be modified for any front-covers that an integrated PV module may have using Eq. 3, which in the case of this study is a clear solar glass. Here G_{x0} is the initially calculated irradiance for the sensor point, either direct or diffuse. For f_{loss} a factor is dependant on the colouring

[1] https://www.energy.ca.gov/media/2367

[2] Implementation of the PCA and K-Medoids are from the Python library *scikit-learn*

[3] parameters: -ab 5 -ad 50000 -as 4096 -c 1 -dc 0.75 -dp 512 -dr 3 -ds 0.05 -dt 0.15 -lr 8 -lw 2e-07 -ss 1.0 -st 0.15

https://doi.org/10.52202/069564-0306

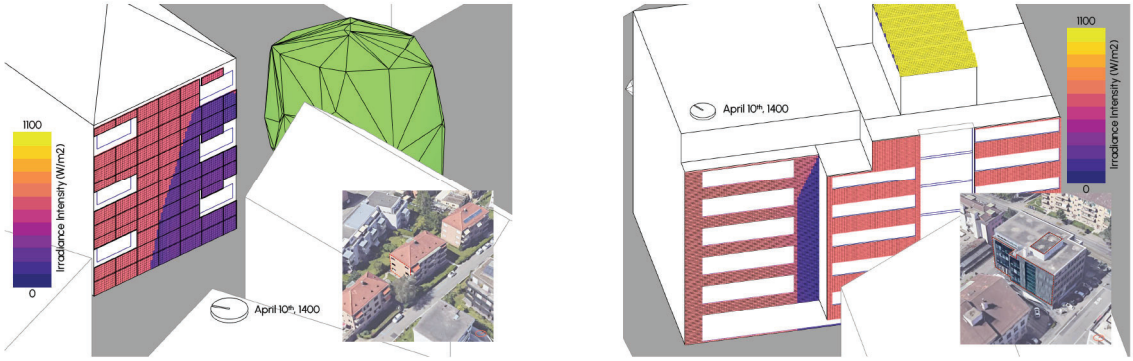

Figure 2: The two archetypal façades and unobstructed roof (highlighted) used in the study are shown next to their 3D models. In (a) we utilise a lower rise building in the district with a moderately obstructed facade and nearby vegetation. In (b) we utilise a larger facade with more obstruction.

of the front cover and comes from [30].

$$G_x = G_{x0} \cdot (1 - f_{loss}) \tag{3}$$

To calculate G_{eff} for each sensor point we account for the reflectivity of the glass and front cover with an angle of incidence modifier (AOI), shown in Eq. 4 for each timestep based on the location, orientation of the surface, and tilt of the surface.

$$G_{eff} = G_{dir} K(\Theta) + G_{diff} K(60^\circ) \tag{4}$$

K is the angular response factor calculated following Martin and Ruiz (2001) [31], formulated in Eq. 5. K is dependent on Θ and a dimensionless fitting parameter, a_r, which is fixed at 0.17.

$$K = \frac{e^{\frac{1}{a_r}} \left(1 - e^{\frac{\cos(\Theta)}{a_r}}\right)}{e^{\frac{1}{a_r}} - 1} \tag{5}$$

Given G_{eff} of each sensor point, the power conversion model for each hour of the year, shown in Eq. 6, is based on the nominal efficiency of the module(η_{nom}), total surface area available for modules (*area*), and a performance correction dependant on the maximum power temperature coefficient of the module (γ_{ref}) and cell or module temperature (T_{sensor}) which comes from Eq. 1. In this instance we calculate *area* by subtracting the area of windows found within each discretized section the façade from the area of the section. We account for losses in the system due to soiling, cabling, and inverter loss using I_{misc}, which is fixed at 0.10.

$$P_{AC} = \left(\frac{G_{eff}}{G_{stc}} \cdot P_{peak} \cdot [1 + \gamma_{ref} (T_{sensor} - T_{stc})]\right) \cdot (1 - I_{misc}) \tag{6}$$

For the surface-based analysis we calculate P_{peak} using Eq. 7 where $P_{nameplate}$ denotes the standard module capacity, $C_{nameplate}$ denotes the number of cells in a standard module, $A_{nameplate}$ denotes the area of the standard module, and A_{face} denotes the area associated with sensor point in the discretized surface:

$$P_{peak} = \frac{P_{nameplate}}{C_{nameplate}} \cdot \frac{C_{nameplate}}{A_{nameplate}} \cdot A_{face} \tag{7}$$

3.4. Module-based framework

To represent another existing approach to modeling the performance of PV in urban arrays we evaluate simulated performance of modules placed into the surfaces analysed in the previous method. The modules are assessed using a single irradiance sensor point located at the module's center and the power conversion model of Eq. 6, with the only difference being the input for P_{peak} where we employ each module's unique size. The modules are created in a 3D model of the surface which begins by assuming that no windows or impediments exist on the surface. Where they does exist the modules are cut into smaller rectangles. Then we replace A_{face} in Eq. 7 with the area of each individual module.

3.5. Cell-based framework

We increase the resolution of the previous framework by calculating power for the center point of each cell in the array's modules using Eq. 6. The modules modeled in the previous framework are discretized by the cell dimensions, frame width, and spacing between the frame. The input for A_{face} in Eq. 7 is then calculated based on the cell dimensions.

3.6. IV curve-based framework

In this section we describe the proposed modeling framework for high-resolution BIPV analysis that is the focus of this paper. Given the spatially discretized grid from the previous approach we improve the model resolution here by changing the power model. We build on an existing approach for cell-based modeling found in Walker et al. [24]. With this approach we have included a more flexible input for the module type that enables the use of module sizes that are non-standard, which is common in BIPV design and occurs in the 3D models being assessed in this study. With the modules and cells modeled in the 3D space, string connections of modules are built up by first grouping modules of the same cell count into strings. Then the string with the standard module size is split into separate strings with each string having the same modules of the same vertical height. In preparation for the power calculation, each module is assigned four numerical arrays. The first contains the Cartesian position of each cell's center point. The second contains the surface normal of the cells. The third represents to which bypass diode in the module that each cell belongs to. The final is used if a module has multiple sub-modules in parallel, such as in a Half-Cut module, and represents to which sub-module each cell belongs.

G_{eff} is calculated in the same way as the previous framework but is applied to a different power model. The power conversion model is more detailed in this approach as we calculate the IV-curve for each cell. Then, the module IV-curve is compiled based on bypass diodes and string or parallel connections. With each module's IV characteristics, we evaluate the arrays for several electrical topologies: micro-inverter, string inverter, central inverter.

The initial IV-curve for a cell is calculated following Bishop (1988) [4], using Eq. 8. This formulation follows the common single-diode equivalent circuit model that is also applied by EnergyPlus [16] and in the method of Walker et al. (2019) which we build upon. It is assumed that a single cell can be modeled as a portion of the larger module. This is important as the parameters necessary for the single-diode model are typically only given for a module as it was characterised during manufacturer testing. This approach uses the five-parameter input from De Soto et al. (2006) [32]. This uses G_{eff}, T_{cell} (which comes from Eq. 1), the short-circuit temperature coefficient (α_{sc}), diode ideality factor (n_D), number of cells in series (N_{s}), the thermal voltage across the cell (V_{th}), light generated photocurrent at reference conditions ($I_{\text{L,ref}}$), diode reverse saturation current at reference conditions ($I_{0,\text{ref}}$), shunt resistance at reference conditions ($R_{\text{sh,ref}}$), and series resistance at reference conditions ($R_{\text{s,ref}}$). The calculations provided by De Soto et al. produce the diode voltage (V_{d}), photocurrent (I_{L}), saturation current (I_0), series resistance (R_{s}), shunt resistance (R_{sh}), and $nNsVth$. We use the default parameters for breakdown factor (a, 0.0), breakdown voltage (V_{br}, -5.5), and the breakdown exponent (m, 3.28). We include $\frac{d^2}{\mu\tau}$ for completeness, but it is not used in this study as it is only relevant for amorphous silicon cells, therefore it is assigned a value of 0. With the parameters assembled the IV-curve is calculated for each cell, envisioning it as a single module. The resulting curve's V values are divided by the number of cells in series and the I values are divided by the number of cells in parallel.

$$I = I_{\text{L}} - I_0 \left(\exp \frac{V_{\text{d}}}{nN_s V_{\text{th}}} - 1 \right) - \frac{V_{\text{d}}}{R_{\text{sh}}} - \frac{I_{\text{L}} \frac{d^2}{\mu\tau}}{N_s V_{\text{bi}} - V_{\text{d}}} - a \frac{V_{\text{d}}}{R_{\text{sh}}} \left(1 - \frac{V_{\text{d}}}{V_{\text{br}}} \right)^{-\text{m}} \tag{8}$$

This model enables the characterisation of the cell in the second quadrant of the IV-curve plot. This is the characterisation of the reverse-bias potential of the cell. If two cells with mismatched curves are connected in series and operated with the more illuminated cell's maximum power potential, then the less illuminated cell will draw current from the first cell. Thus, the real operation of these cells would require the more illuminated cell to be operated at the level of the lower cell, limiting maximum power potential (MPP). It is this phenomenon that is common in partial shading and we suspect is not well captured in the other three frameworks. Using this approach all cell IV-curves are calculated and first connected in series within each diode pathway, following Kirchoff's circuit laws. Then the various diode pathways of a module are connected in series. If parallel connections exist within the module then these are made to finalise the characterisation of each module's IV-curve.

From here the approach branches to simultaneously evaluate performance of the array using multiple electrical topologies. This is essential for properly characterising MPP in each module as explained earlier, devices under different illumination can limit each other to avoid reverse-bias.

First, individual modules are evaluated using a micro-inverter approach where DC to AC inversion occurs

https://doi.org/10.52202/069564-0306

along with the maximum power point tracking (MPPT). Then, using the same principles of series and parallel connection within the module, strings of modules are connected and the MPPT and inversion is applied to extract MPP for each string. Lastly, strings are connected in parallel to evaluate their power using a single central inverter. We apply a simple 95% inverter efficiency to all inverter operations.

4. Results & Discussion

Here we present and analyse the results of the two portions of the study. First, the proposed modeling framework is evaluated alongside a measured dataset. Second, the simulation results of the proposed framework and surface-based framework are compared.

4.1. Evaluation of High-Resolution Proposed Framework

Figure 3 describes the two power outputs against G_{eff} with a linear curve fitted to the data scatter. Qualitatively, we observe generally good agreement between the two models at lower irradiance levels. However, with higher irradiance levels the proposed model produces a larger P_{DC} response. MAE and root mean squared error (RMSE) of the two data sets is 0.73 kWh, and 1.41 respectively. Additionally, we do not observe in the modeled data very low P_{DC} response at high levels of irradiance, such as seen in the measurement data. We suspect that in this case that much of the measurement array was covered by a shadow, but the censor cell was not. Despite these points the standard deviation and variance of the measurement dataset is lower than that of the model output.

The lack of multiple sensors throughout the array impedes our ability to model the array under heterogeneous conditions, which is likely closer to reality. Factors such as cloud cover that may cover much of the array while the sensor cell is still directly illuminated would then not be captured by the model. This could lead to the over prediction that we witness. Additionally, the proposed framework is meant for vertical facades in an environment with a lot of shading and a only slightly ventilated air cavity between the model and mounting surface. A dataset that contains these attributes would be a better tool to evaluate and eventually validate the proposed framework.

4.2. Comparison of Modeling Frameworks

Here we compare the outputs of the modeling frameworks and discuss their implications for use in larger models. First we evaluate the received irradiance for each framework. Irradiance results for each framework are influenced by the number of sensor points available to the ray-tracing simulation as this allows the ray-tracing to more accurately depict objects that might shade the receiving surface. In Figures 4a-4c we show difference between the irradiance, normalised by available surface area, levels across both of the 3D models through their probability distribution functions. A trend emerges with each in that the *Cell Center* and *Cell IV* framework have overlapping curves, while the *Surface Face* is closely aligned, and the *Module Center* framework contains a time series of larger values. This is due to the self-shading of the array not being captured by the center point on the module, whereas in the *Cell Center* and *Cell IV* a shared sensor grid is used that has many points. The close alignment of the *Surface Face* model is interesting, due to it having many less sensor points. This is worthwhile for future research.

In Figure 5a we show the discretized modules of the Commercial Building's rooftop array. The selected date was chosen for being the hour of the year with the maximum variance amongst the G_{eff} values within each modules, the value being indicated in Table 2. We can see that for the majority of the modules there is a shaded section caused by the module in front. This leads to a high degree of variance across the module. In the case of the *Module Center* the shaded portion of the module is not captured as only the central point is

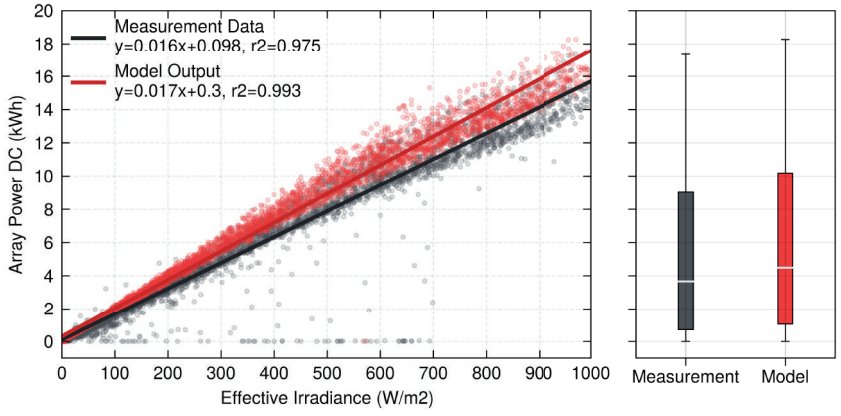

Figure 3: Linear regression of measurement and modeled data where $G_{\text{eff}} > 0$.

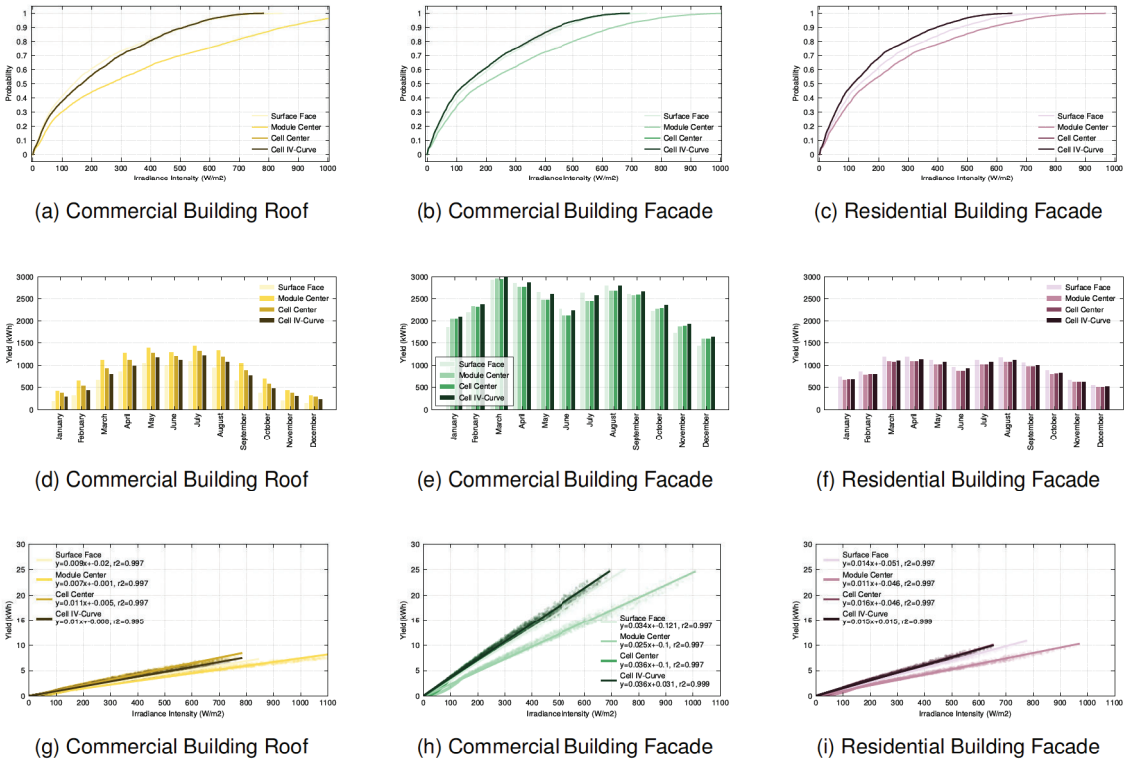

(a) Commercial Building Roof (b) Commercial Building Facade (c) Residential Building Facade

(d) Commercial Building Roof (e) Commercial Building Facade (f) Residential Building Facade

(g) Commercial Building Roof (h) Commercial Building Facade (i) Residential Building Facade

Figure 4: Comparison of the results of the simulations for each of the frameworks. (a-c) The probability distribution function for the irradiance intensity time series (8760 hours) for each of the three surfaces examined. (d-f) Yield comparison resampled for monthly sums. (g-i) Linear regression of the irradiance intensity of the module and the yield for each framework on the three arrays.

sampled to calculate G_{eff}. This inability to capture self-shading extends to the *Surface Face* framework as well, but due to the lack of rotation of the face the total irradiance available to these surfaces is limited anyway.

Looking at the other arrays in Table 2 we see some degree of variance across the modules but with means around 1 and 3 $\frac{W}{m^2}$. This contributes to the yield of the arrays being more consistent amongst the different frameworks, shown in Figures 4e-4f.

Simpler models such as the *Module Center* of *Cell Center* could be used in place of the much more computationally expensive *Cell IV* approach if the conditions for shading are met. In Figures 4g-4i we show linear regression of yield and irradiance intensity on the module. As the variance found in the Commercial Facade and Residential Facade are quite low the regressed models fit the data well. While still a good fit, the lowest r^2 is seen in the *Cell IV* framework of the Commercial Rooftop where, the regression is fit to a wider spread of data points. For the same levels of irradiance intensity different levels of yield are found. This is because the plot shows the irradiance intensity across the entire array, and does not reflect the activity in the modules under mismatch conditions. The results shown for the *Cell IV* framework are those for a system with micro-inverters. This type of electrical topology is able to handle the mismatch conditions well as maximum power (MP) tracking occurs at the module level. We show in Figure 5b the same array conditions in Figure 5a. Here the string inverter system controls the MP of each row of modules independently while the central inverter controls the MP of all modules. We see a drop in the yield if the system is configured with a central inverter due to the need of the system to operate the southern-most row of modules at the same level as the other strings.

Computationally speaking the *Cell IV* approach requires the most setup, although all require the same 3D geometry. From a computational standpoint the *Cell IV* require on average 800 seconds for each simulation of a surface, while the other methods require around 120 seconds.[4]

[4]These numbers come from operating the models on a 2021 Macbook Pro with 8-cores (ARM).

https://doi.org/10.52202/069564-0306

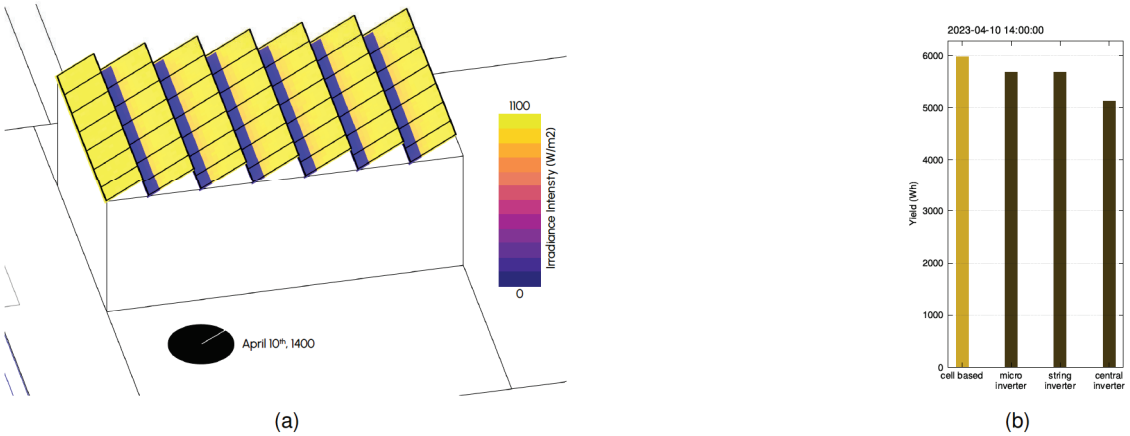

(a) (b)

Figure 5: The irradiance intensity for the rooftop array on the 1st of April at 1400 (a) and the comparison (b) of power output of the array for all three electrical topologies and the *Cell Center* framework

	Commercial Roof	Commercial Facade	Residential Facade
mean	70.355	0.994	3.134
std	76.694	1.363	6.216
min	0.109	0.001	0.004
25%	9.591	0.204	0.345
50%	35.793	0.575	0.94
75%	115.716	1.228	2.087
max	319.586	12.575	55.133

Table 2: The descriptive statistics for the standard deviation found within the effective irradiance (W/m2) for each module's cell points across the year in each of the three arrays.

5. Conclusion

In this paper we proposed a detailed modeling framework for the simulation of building-based PV performance through the characterisation of system-wide IV-curves. This approach is based on existing work in the field with some adjustments to capture a variety of potential electrical topologies. We evaluated this model's performance against measured data and found that the model generally over-predicts, with a mean absolute error of 0.65 kWh. We propose that to better tune the framework a better measurement dataset is needed that can provide a more comprehensive picture of array-wide irradiance and cell temperature characteristics. Additionally, the measurement data should be for vertical arrays under partial shading.

We compared the proposed framework to three common approaches found in the literature. We found that in systems with self shading, the proposed framework is capable of capturing the impact on the modules while surface based and module center based methods are not. The similarly spatially accurate cell center based framework yields similar results, but with less computational expense. The three frameworks found in the literature do not provide a way to compare between electrical topologies, which in the case of partially shaded modules is necessary to evaluate which topology to choose. If you need to analyse different electrical topologies the *Cell IV* framework is necessary.

Beyond this, more research is necessary to compare this framework to the proposed to determine in what cases the more expensive method should be used. We believe though that this suggests that the type of shading cast on the array is important in determining which model is necessary to most accurately predict system yield. Future research should be dedicated to understanding the shading profiles and objects that occlude arrays in order to classify them so we might use the type of shading to select the power conversion model.

Acknowledgments

This research was conducted at the Future Cities Lab Global at ETH Zurich. Future Cities Lab Global is supported and funded by the National Research Foundation, Prime Minister's Office, Singapore under its Campus for Research Excellence and Technological Enterprise (CREATE) programme and ETH Zurich (ETHZ), with additional contributions from the National University of Singapore (NUS), Nanyang Technological University (NTU), Singapore and the Singapore University of Technology and Design (SUTD).

References

[1] Christoph Waibel et al. “Sensitivity analysis on optimal placement of façade based photovoltaics”. In: *Proceedings of the 31st international conference on efficiency, cost, optimization, simulation and environmental impact of energy systems*. ECOS 2018. ISBN: 9789729959646. Guimarães, Portugal: Universidade do Minho., 2018, 12 pp. URL: https://www.dora.lib4ri.ch/empa/islandora/object/empa%3A22695/ (visited on 11/08/2022).

[2] Iris van Beuzekom, Bri-Mathias Hodge, and Han Slootweg. “Framework for optimization of long-term, multi-period investment planning of integrated urban energy systems”. In: *Applied Energy* 292 (2021), p. 14. DOI: 10.1016/j.apenergy.2021.116880. URL: https://doi.org/10.1016/j.apenergy.2021.116880.

[3] Georgios Mavromatidis and Ivalin Petkov. “MANGO: A novel optimization model for the long-term, multi-stage planning of decentralized multi-energy systems”. In: *Applied Energy* 288 (Apr. 15, 2021), p. 116585. ISSN: 0306-2619. DOI: 10.1016/j.apenergy.2021.116585. URL: https://www.sciencedirect.com/science/article/pii/S030626192100129X (visited on 04/11/2022).

[4] J.W. Bishop. “Computer simulation of the effects of electrical mismatches in photovoltaic cell interconnection circuits”. In: *Solar Cells* 25.1 (Oct. 1988), pp. 73–89. ISSN: 03796787. DOI: 10.1016/0379-6787(88)90059-2. URL: https://linkinghub.elsevier.com/retrieve/pii/0379678788900592 (visited on 07/21/2022).

[5] Sergio Castellanos, Deborah A Sunter, and Daniel M Kammen. “Rooftop solar photovoltaic potential in cities: how scalable are assessment approaches?” In: *Environmental Research Letters* 12.12 (Dec. 1, 2017), p. 125005. ISSN: 1748-9326. DOI: 10.1088/1748-9326/aa7857. URL: https://iopscience.iop.org/article/10.1088/1748-9326/aa7857 (visited on 03/06/2023).

[6] SFOE. *Sonnenfassade*. 2020. URL: http://www.sonnendach.ch (visited on 03/29/2022).

[7] Erika Saretta, Pierluigi Bonomo, and Francesco Frontini. “A calculation method for the BIPV potential of Swiss façades at LOD2.5 in urban areas: A case from Ticino region”. In: *Solar Energy* 195 (Jan. 2020), pp. 150–165. ISSN: 0038092X. DOI: 10.1016/j.solener.2019.11.062. URL: https://linkinghub.elsevier.com/retrieve/pii/S0038092X19311624 (visited on 03/13/2022).

[8] JRC. *Photovoltaic Geographical Information System (PVGIS)*. Version 5.2. Mar. 2023. URL: https://re.jrc.ec.europa.eu/pvg_tools/en/ (visited on 03/06/2023).

[9] NREL. *PVWatts Calculator*. Version 8.1.0. Golden, CO, Mar. 2023. URL: https://pvwatts.nrel.gov/ (visited on 03/06/2023).

[10] Thomas Huld et al. “A power-rating model for crystalline silicon PV modules”. In: *Solar Energy Materials and Solar Cells* 95.12 (Dec. 2011), pp. 3359–3369. ISSN: 09270248. DOI: 10.1016/j.solmat.2011.07.026. URL: https://linkinghub.elsevier.com/retrieve/pii/S0927024811004442 (visited on 03/06/2023).

[11] Ronald G. Ross. “Characterization of photovoltaic array performance: An overview”. In: *Solar Cells* 18.3 (Sept. 1986), pp. 345–352. ISSN: 03796787. DOI: 10.1016/0379-6787(86)90133-X. URL: https://linkinghub.elsevier.com/retrieve/pii/037967878690133X (visited on 03/20/2023).

[12] Jimeno A. Fonseca et al. “City Energy Analyst (CEA): Integrated framework for analysis and optimization of building energy systems in neighborhoods and city districts”. In: *Energy and Buildings* 113 (Feb. 2016), pp. 202–226. ISSN: 03787788. DOI: 10.1016/j.enbuild.2015.11.055. URL: https://linkinghub.elsevier.com/retrieve/pii/S0378778815304199 (visited on 03/30/2022).

[13] Christoph Waibel, Ralph Evins, and Jan Carmeliet. “Efficient time-resolved 3D solar potential modelling”. In: *Solar Energy* 158 (Dec. 2017), pp. 960–976. ISSN: 0038092X. DOI: 10.1016/j.solener.2017.10.054. URL: https://linkinghub.elsevier.com/retrieve/pii/S0038092X17309349 (visited on 03/06/2023).

[14] MIT Sustainable Design Lab. *DAYSIM*. original-date: 2016-02-24T16:00:14Z. July 8, 2022. URL: https://github.com/MITSustainableDesignLab/Daysim (visited on 11/23/2022).

[15] LBNL ETA. *Radiance*. Version 5.3. Golden, CO, Sept. 2020. URL: https://github.com/LBNL-ETA/Radiance/releases/tag/012cb178.

[16] NREL. *EnergyPlus*. Version 22.2.0. Golden, CO, Mar. 2023. URL: https://github.com/NREL/EnergyPlus/releases/tag/v22.2.0 (visited on 03/06/2023).

[17] Jay Kratochvil, William Boyson, and David King. *Photovoltaic array performance model*. SAND2004-3535, 919131. Aug. 1, 2004, SAND2004–3535, 919131. DOI: 10.2172/919131. URL: https://www.osti.gov/servlets/purl/919131/ (visited on 03/06/2023).

https://doi.org/10.52202/069564-0306

[18] K. Sinapis et al. “A comprehensive study on partial shading response of c-Si modules and yield modeling of string inverter and module level power electronics”. In: *Solar Energy* 135 (Oct. 2016), pp. 731–741. ISSN: 0038092X. DOI: 10.1016/j.solener.2016.06.050. URL: https://linkinghub.elsevier.com/retrieve/pii/S0038092X16302316 (visited on 03/14/2022).

[19] Chris Tzikas and Gabriela Gómez. “Do Thin Film PV Modules Offer an Advantage Under Partial Shading Conditions?” In: *Proceedings of the 33rd European Photovoltaic Solar Energy Conference and Exhibition*. European Photovoltaic Solar Energy Conference and Exhibition. Amsterdam, the Netherlands: EU PVSEC, Nov. 2017, p. 5.

[20] Simon Ravyts et al. “Impact of photovoltaic technology and feeder voltage level on the efficiency of façade building-integrated photovoltaic systems”. In: *Applied Energy* 269 (July 2020), p. 115039. ISSN: 03062619. DOI: 10.1016/j.apenergy.2020.115039. URL: https://linkinghub.elsevier.com/retrieve/pii/S0306261920305511 (visited on 03/27/2022).

[21] Konstantinos Spiliotis et al. “Electrical system architectures for building-integrated photovoltaics: A comparative analysis using a modelling framework in Modelica”. In: *Applied Energy* 261 (Mar. 2020), p. 114247. ISSN: 03062619. DOI: 10.1016/j.apenergy.2019.114247. URL: https://linkinghub.elsevier.com/retrieve/pii/S0306261919319348 (visited on 03/14/2022).

[22] Bennet Meyers and Mark Mikofski. “Accurate Modeling of Partially Shaded PV Arrays”. In: *2017 IEEE 44th Photovoltaic Specialist Conference (PVSC)*. 2017 IEEE 44th Photovoltaic Specialist Conference (PVSC). June 2017, pp. 3354–3359. DOI: 10.1109/PVSC.2017.8521559.

[23] Chetan Chaudhari et al. “Quantification of System-Level Mismatch Losses using PVMismatch”. In: *2018 IEEE 7th World Conference on Photovoltaic Energy Conversion (WCPEC) (A Joint Conference of 45th IEEE PVSC, 28th PVSEC & 34th EU PVSEC)*. 2018 IEEE 7th World Conference on Photovoltaic Energy Conversion (WCPEC) (A Joint Conference of 45th IEEE PVSC, 28th PVSEC & 34th EU PVSEC). ISSN: 0160-8371. June 2018, pp. 3626–3629. DOI: 10.1109/PVSC.2018.8548107.

[24] Linus Walker, Johannes Hofer, and Arno Schlueter. “High-resolution, parametric BIPV and electrical systems modeling and design”. In: *Applied Energy* 238 (Mar. 2019), pp. 164–179. ISSN: 03062619. DOI: 10.1016/j.apenergy.2018.12.088. URL: https://linkinghub.elsevier.com/retrieve/pii/S0306261918319044 (visited on 03/14/2022).

[25] Matthew T. Boyd. *High-Speed Monitoring of Multiple Grid-Connected Photovoltaic Array Configurations*. NIST TN 1896. National Institute of Standards and Technology, Oct. 2015, NIST TN 1896. DOI: 10.6028/NIST.TN.1896. URL: https://nvlpubs.nist.gov/nistpubs/TechnicalNotes/NIST.TN.1896.pdf (visited on 03/08/2023).

[26] Filip Biljecki and Yoong Shin Chow. “Global Building Morphology Indicators”. In: *Computers, Environment and Urban Systems* 95 (July 2022), p. 101809. ISSN: 01989715. DOI: 10.1016/j.compenvurbsys.2022.101809. URL: https://linkinghub.elsevier.com/retrieve/pii/S0198971522000539 (visited on 11/08/2022).

[27] Robert McNeel \& Associates. *Rhinoceros 3D*. Version Rhino 7.18.22145.08132. May 25, 2022.

[28] Giuseppe Peronato, Emmanuel Rey, and Marilyne Andersen. “3D model discretization in assessing urban solar potential: the effect of grid spacing on predicted solar irradiation”. In: *Solar Energy* 176 (Dec. 1, 2018), pp. 334–349. ISSN: 0038-092X. DOI: 10.1016/j.solener.2018.10.011. URL: https://www.sciencedirect.com/science/article/pii/S0038092X18309861 (visited on 03/13/2022).

[29] Sarith Subramaniam. *Daylighting Simulations with Radiance using Matrix-based Methods*. Berkeley: LBNL Energy Technologies Area, Oct. 2017.

[30] Arne Røyset, Tore Kolås, and Bjørn Petter Jelle. “Coloured building integrated photovoltaics: Influence on energy efficiency”. In: *Energy and Buildings* 208 (Feb. 2020), p. 109623. ISSN: 03787788. DOI: 10.1016/j.enbuild.2019.109623. URL: https://linkinghub.elsevier.com/retrieve/pii/S0378778819322091 (visited on 03/16/2022).

[31] N. Martin and J. M. Ruiz. “Calculation of the PV modules angular losses under field conditions by means of an analytical model”. In: *Solar Energy Materials and Solar Cells* 70.1 (Dec. 1, 2001), pp. 25–38. ISSN: 0927-0248. DOI: 10.1016/S0927-0248(00)00408-6. URL: https://www.sciencedirect.com/science/article/pii/S0927024800004086 (visited on 07/12/2022).

[32] W. De Soto, S. A. Klein, and W. A. Beckman. “Improvement and validation of a model for photovoltaic array performance”. In: *Solar Energy* 80.1 (Jan. 1, 2006), pp. 78–88. ISSN: 0038-092X. DOI: 10.1016/j.solener.2005.06.010. URL: https://www.sciencedirect.com/science/article/pii/S0038092X05002410 (visited on 03/29/2022).